Electrodilatometric analysis under applied force: A powerful tool for electrode investigation

Electrodilatometric analysis under applied force: a powerful tool for electrode investigation

Giampaolo Lacarbonara[a,§], Morteza Rahmanipour[a,#,§], Juri Belcari[b,c], Lorenzo Lodi[c], Andrea Zucchelli[b], Catia Arbizzani[a,*,§]

[a]Alma Mater Studiorum - University of Bologna, Dept. of Chemistry "Giacomo Ciamician", Via F. Selmi 2, 40126 Bologna, Italy

[b]Alma Mater studiorum - Engineering School, Industrial Engineering Department (DIN), Viale del Risorgimento 2, 30136, Bologna, Italy

[c]Marposs Spa Italy, Via Saliceto, 13, 40010 Bentivoglio (Bo), Italy

* Corresponding Author: catia.arbizzani@unibo.it

§ ISE Members

Present address: Manz Italy Srl, Via S. Lorenzo, 19, 40037 Sasso Marconi (BO), Italy

Abstract

A new equipment for in situ electrochemical dilatometry is designed and validated by studying the volumetric changes of a model electrode. The contactless measurement system permit to not influence the dilation of the sample during the tests. In addition, different forces can be applied in a selected range. Graphite is selected as model electrode and electrochemical tests in different electrolytes are carried out under different applied forces.

The results of the electrodilatometric tests on graphite in EC:DMC- and in PC-based electrolyte reveal not only lithium insertion/deinsertion process, but also the presence of simultaneous phenomena like solvent evaporation, SEI formation and gas evolution. The latter has been

detected by applying different forces that affect the gas uptake and release from porous separator.

We demonstrate that with this new equipment it is possible, from thickness variation, to collect information on processes of different nature in addition to the lithiation/delithiation. Specifically, different applied forces emphasized gas evolution, which is a worth studying phenomenon for increasing battery safety.

Keywords

In-situ dilatometry, lithium-ion batteries, exfoliation, graphite, gassing.

1. Introduction

The necessity of an energy transition and the development of new renewable power sources needs the support of competitive energy storage systems. The advantages of the development of this field allow for tying the new power sources to the grid, making the unpredictable behaviour of renewable sources overcome. In the electrical energy storage panorama, batteries and supercapacitors play a key role for their modularity and efficiency [1].

In many types of batteries, such as the Li-ion battery family, the faradic processes involve reversible insertion of ions in the lattice of the electrodes. The insertion of ions often implies changes in volume and in some cases, huge expansion of the electrodes. The magnitude of this phenomenon depends on the available hosting position and on the dimensions of the guests. While lithium insertion in $LiFePO_4$ results in an expansion of 6.8 %, sodium insertion in $NaFePO_4$ leads to a thickness increase of 12.8 % [2].

Uncontrolled expansions can lead to failure and damages to the materials such as exfoliation in layered materials [3] or irreversible shrinking in insertion materials [4].

Hence, the study of volumetric stability of the electrodes under cycling is fundamental to detect materials damage, to better analyze consequent materials failure, to precisely predict the lifetime and long-term stability of the cell and to improve battery safety [5].

In situ electrochemical dilatometry can be used to record macroscopic expansion and contraction of materials during reactions in combination with electrochemical techniques.

This technique is especially useful to evaluate those systems in which volume changes lead to mechanical degradation or formation of unstable solid electrolyte interphase (SEI) that can severely affect safety [6–9]. In situ dilatometry allows making mechanicistic studies in systems characterized by several intermediate species as in composite sulphur/carbon electrodes adopted in lithium-sulfur batteries [10,11].

In previous works [11–18], in situ dilatometry allowed the monitoring and predicted the behaviour of systems. To this purpose, it is useful to have any leeway to test cells and get different information. The present study aims to test a novel electrochemical dilatometer which can detect the volume variation during an electrochemical experiment with the additional feature of applying controlled pressure on the cell. This new system enables the control of the force in a broad range of values and the detection of the volumetric changes of electrode materials in different conditions. The other features of the new dilatometric equipment under study are: i) the contactless system for the detection of thickness variation, which increases the precision, having the inductive magnetic a measuring range of 500 µm, a resolution of 0.01 µm with a maximum non-linearity error of 0.1 µm; ii) the sealed cell holder that can easily be brought in drybox for cell assembly and, hence, mounted in the dilatometer that remain in ambient atmosphere or in an oven for measurement at different and constant temperatures; iii) the temperature compensation system for measurements from -10°C to 60°C; iv) the cell holder hosting electrodes of different diameter up to 20 mm; v) the applied force range could be changed during the retooling of the system.

The study of well-known electrode models with diverse electrolytic mixtures during cyclic voltammetry cycles validate the performance of this novel apparatus that could be used to evaluate the phenomena occurring during insertions processes such as SEI formation, gas evolution, solvent evaporation, and exfoliation under different applied forces.

2. Experimental Section

2.1 Materials and methods

Graphite electrodes (35 µm thickness) were used as working electrodes (WE) consisting of 90 wt% graphite MAGE (>200 nm, Hitachi), 7 wt% PVDF – Solef S130 (Solvay), 2 wt% Super C-65 (TIMCAL) and 1 wt% graphite SFG6L (6.8 µm, TIMCAL).

Activated carbon electrodes used as counter electrodes (CE) were made by mixing 83.9 wt% carbon PICACTIF (2315 m^2 g^{-1}, 10 µm particle size), 4.6 wt% of carbon Super P (Erachem Comilog N.V.), 4.8 wt% di carboxymethylcellulose sodium salt (Na-CMC, Sigma-Aldrich), 6.7 wt% Teflon® suspension in water (DuPont, solid content of 60.2 wt%) and 500 µL absolute ethanol (Sigma-Aldrich, ≥99.8 wt%).

The separator was a glass fibre membrane (Whatman; Grade: GF/A, 10 mm diameter, 185 µm thickness).

The electrodes and separators were cut into discs with diameters of 9 mm and 10 mm, respectively, by punching, and dried under dynamic vacuum in Büchi B-585 oven at 120 °C for 12 h before assembly.

2.2 Cell Assembly

The electrolytes used were 1 M $LiPF_6$ in 1:1 (w:w) ethylene carbonate (EC): dimethyl carbonate (DMC) (LP30, Selectilyte BASF, Germany) and 1M lithium bis(trifluoromethanesulfonyl)imide (LiTFSI, ≥99.0%, Sigma Aldrich, Germany) in bidistilled

propylene carbonate (PC, ≥99%, Fluka). The thickness of the electrodes was measured using a digital micrometre and by the reference bench of the dilatometer.

The dilatometer cell assembly was performed under argon atmosphere in an MBraun Labmaster SP dry box (H_2O and O_2 < 0.1 ppm) and the measurements started 2 hours after the assembly. Also, T-shaped Teflon® cells (Bola, Bohlender GmbH) with Li reference electrode (RE) were assembled for the evaluation of the electrode potentials while the cell was working in a two-electrode mode like in the dilatometric experiments.

2.3 Chemical-physical measurements

Scanning electron microscopy images (SEM) were captured with a Zeiss EVO 50 and the Raman spectra were recorded using a RENISHAW Mod. INVIA with an Argon ion laser (λ_{exc} 514 nm) as the excitation source. The samples were washed in DMC or PC, according to the solvents used for electrodilatometric tests, to remove salt. DMC was finally used to remove EC and PC, respectively, before SEM and Raman analyses.

2.4 Dilatometric and electrochemical tests

A dilatometer (Marposs S.p.A., Bentivoglio, Italy), equipped for cell testing, was used to measure the volume changes during charge/discharge cycles in electrochemical cells. For the electrochemical measurements, the dilatometer was connected to a PAR273A potentiostat/galvanostat and a Solartron SI 1255 frequency response analyser interfaced with the potentiostat. Dilatometric response was recorded during cyclic voltammetry tests at room temperature, with the cell internal and external temperature measured by the equipment sensors in real-time operations. The electrochemical impedance spectra were recorded in the range of 100 kHz-100 mHz, 10 points/decade with a perturbation amplitude of 5 mV for monitoring the cell behaviour.

3. Results and Discussion

The dilatometric equipment was designed and build by Marposs SpA. It is composed of a solid steel structure, a measuring system for the sample volume variations, a manual adjusting system for tuning of acting force on the sample and a removable sealed sample holder, is equipped with electronics for sensors reading and acquisition, as shown in Figure 1. A contactless measuring system detects the volume changes minimizing the influence of the gauge on the measure itself and that of the expansion of the sample during the tests. The inductive magnetic gauge used has a measuring range of 500 µm, a resolution of 0.01 µm with a maximum non-linearity error of 0.1 µm. Two temperature sensors continuously detect the internal temperature of the cell and the external temperature. Through a ring nut, it's possible to adjust the force acting on the sample under test in a range from about 10 N to 100 N: this peculiarity is very useful in the study of batteries where this parameter is crucial. The sample holder can be easily removed and reassembled on the instrument when dry-box setup operations are needed. The interface displays to the user the instantaneous values of the sensors. Moreover, it allows to configure an acquisition file for their saving and future analyses. The dilatometric equipment is able to record the total deformation of the cell. Nevertheless, we succeed to distinguish the different contribution of the cell components by using a positive electrode that doesn't change too much its dimension because it undergoes capacitive charge/discharge processes. In addition, we started the test after 2 hours, when all the materials had reached a stable thickness.

The reliability of this new dilatometric equipment was experimentally evaluated by using model electrodes with well-established electrochemical processes. In particular, the dilatometric behaviour of graphite electrodes in two different electrolytes has been tested. EC-based electrolytes are well-known for their good compatibility with graphite. EC shows excellent filming capabilities that ensure the formation of a good and stable SEI and DMC decreases the viscosity of the solvent mixture. EC-DMC containing $LiPF_6$ salt is a standard electrolyte

(LP30) due to the broad electrochemical stability and high ionic conductivity as well as to the good protection of the most common aluminium current collector [19, 20]. On the contrary, the cointercalation of PC with lithium ions in graphite leads to a dramatic exfoliation of the electrode [21]. In the absence of additives with filming capabilities, graphite exfoliation occurs at less than 0.9 V vs Li^+/Li without wrecking the bulk structure completely but bringing progressive changes in surface structure [22]. This degradation makes this electrolyte unsuitable for most graphite-based LIBs. In the following paragraphs, the dilatometric results of Li^+ intercalation in graphite will be described in EC:DMC-based electrolytes and compared with those in PC-based ones under an applied force.

3.1 Deformation of the cell components under 10 N

Information about the strain response to controlled applied stresses associated to an electrochemical system gave the possibility to get information about the importance of the deformation of materials on the thickness variation observed during electrochemical experiments. The thickness of the different cell components was monitored in the electrochemical chamber of the dilatometer under a force applied of 10 N (157 kPa for 9 mm disc and 127 kPa for 10 mm disk) by adding LP30 electrolytic solution or PC-1M LiTFSI (150 µL for the full cell and 75 µL for the cell components).

Under the applied pressure, all the materials respond with a deformation that leads to a fast decrease of thickness in the first 2 hours (Figure 2). Absolute and percentual thickness variation of the cell components in LP30 are reported in Figure 2a and 2b. The separator and the CE showed the smallest thickness decrease around 13.0 µm (-9.2 %) and 2.6 µm (-0.7 %) after 14 hours, respectively. This behaviour was expected for CE. The selection of a CE based on activated carbon, indeed, was done on the basis of its capacitive properties. It accumulates charge without ion insertion in the electrode bulk active mass, limiting the electrode deformation.

On the other hand, the graphite electrode showed higher deformation that stabilizes after 14 hours (-123 % with respect to the dry electrode). Such a high thickness variation could be justified by the increased thickness of the wet electrode taken as starting reference value. The electrode wetting and related thickness change deserve further investigation. In LP30, indeed, both DMC evaporation and graphite deformation act on swelled materials.

The cell deformation (52 μm, -9.2%) was smaller than the sum of the variation of the individual components. It is reasonable that the stress induced by the applied force was distributed on the various components and causes the deformation mostly on the weakest material.

In PC-based electrolyte (Figure 2c and 2d), the less deformable materials (after 14 hours) were again the separator and the CE with 3.7 μm (2.9 %) and 7.3 μm (1.8 %), and the graphite electrode showed the highest deformation, around 11.8 μm (25 %). The thickness variation observed in LP30 electrolyte compared with that of the same components in PC suggests that the recorded compression could depend both on the deformation of the materials and on the presence of DMC that evaporates, evidenced by salt traces in the cell holder. Indeed, in the PC-based electrolyte, the magnitude of the deformation of all materials is three up to five times lower. With the PC-based electrolyte, it is possible to assume that the response observed is entirely due to the compression of the examined materials.

The highest deformation in graphite results also predictable if correlated to the softness of the materials itself due to the weak π-π stacking interactions between the graphitic layers. By combining graphite with the stable activated carbon CE, it is likely that the former mostly originates thickness variations in the full cell.

3.2 EC: DMC-based electrolyte

The voltage window of the electrodilatometric tests has been set after having monitored the electrode potentials vs Li in a Bola cell during cyclic voltammetry (CV) carried out in 2-

electrode mode for simulating the experiments in the dilatometer cell holder (see Figure S1 and Table S1).

After getting an insight about the pressure effect on the samples as previously described, and having established the potential window, the dilatometric tests were carried during CVs at 2 mV s^{-1} and under an applied force of 10 N. The assembled cell showed an OCV of -74 mV.

The CV showed in Figure S2 is entirely reproducible with the one obtained in the T-shaped cell experiment (Figure S1). In Figure 3a are reported the thickness variation (red) and the current (gray) during the first two CVs with the cell voltage on the top axis. The grey vertical lines indicate the cut-off voltages of the CV. The dilatometric profile is characterized by small expansion/shrinking peaks (less than 1 μm) originated from the reduction/oxidation of the graphite electrode and the corresponding insertion/deinsertion of lithium ions within the graphitic layers. The expansions begin close to a cell voltage of – 3 V that corresponds to ≈ 0.6 V vs Li^+/Li.

Additionally, a significant expansion that raises the baseline was observed over the initial ten CV cycles (Figure 3b). The expansion was ascribed to the gas evolution due to the decomposition of EC during the SEI formation as discussed in detail in Section 3.4. The thickness increase due to the gassing phenomena partially covers the thickness variations during insertion/deninsertion processes. It is partially compensated by the thickness decreasing phenomena due to the compression of the cell components under 10 N force as reported in Figure 2.

3.3 PC-based electrolyte

The potential window of the electrode materials in 1 M LiTFSI in PC has been set by monitoring the electrode potentials vs Li reference electrode in the same configuration reported in section 3.2. The electrode potential values were very similar to those reported for LP30 in Table S1.

The experiments in PC-1 M LiTFSI were performed in two different potential ranges with the lower graphite potential limited to 0.9 V vs Li^+/Li to restrains the exfoliation of the graphite, or set to ≈ 50 mV vs Li^+/Li for reaching the exfoliation condition.

Figure 4a demonstrates the thickness variation (red) and the current (gray) during the first two CVs with the cell voltage on the top axis. The grey vertical lines indicate the cut-off voltages of the CV. The dilatometric profile shows bigger expansion/shrinking peaks than those in LP30. The expansion/shrinking peaks aligned with the insertion/deinsertion of lithium-ion in the layered material are reversible in accordance with the imposed cell voltage that prevents the complete exfoliation of the material. The progressive decrease of the baseline observed in Figure 4b retraces the temperature variation (reported in blue) during the experiments that were carried out at room temperature.

3.*4 Variable forces experiment*

SEI formation mechanisms often involve the release of gas-phase products such as CO_2, H_2, CO, and $C_{n<3}$ hydrocarbons [23]. As reported in Scheme 1, in EC/DMC mixtures the reduction of EC and DMC to form lithium alkylcarbonate compounds produces hydrocarbons as co-products. In particular, Liu and co-workers [24] determined by in situ differential electrochemical mass spectroscopy (DEMS) measurements that the main gases originated during SEI formation on graphite electrodes in the first cycle are ethylene and CO_2 [25–27]. Bernard et al.'s investigation on graphite electrode with on-line DEMS reveals that the first negative scan leads to a breakdown of the 0.3% of the total amount of EC in 1M EC: diethyl carbonate (DEC) 3: 7 wt%). In the reported condition, that corresponds to 0.293 μmol of EC [28] that decomposes to give 0.15 μmol of propylene.

In order to make considerations about gassing in common alkyl-carbonate electrolytes, controlled hydrogen evolution experiments were carried out at different applied forces in order to assess the gassing detection ability of the dilatometer.

In a chronoamperometric experiment, 1 V was applied between two platinum electrodes and, H_2 evolution occurs. The micromolar amount of evolved hydrogen was detected as a slight raising (0.6 μm) of the thickness variation curve that stops when the chronoamperometry ends. From the integral of the current curve over time, the amount of 5 μmol of H_2 was estimated to be produced during the test. Given that the temperature was constant, the thickness variation observed was ascribable to the gas formed. By increasing the force up to 20 N, the entity of the observed expansion decreases from 0.6 μm to 0.3 μm, even if the amount of H_2 produced was higher (≈ 25 μmol), as shown in Figure 5a and 5b. In these experiments, the pressure resulting from the hydrogen evolution is not enough to contrast the applied force. However, the behaviour at 20 N leads us to suggest a mechanism in which the gas formed can be trapped by the porous separator that amplifies the thickness response. The application of a higher force decreases the porosity of the separator and less H_2 can be trapped inside the pores, thus justifying the lower thickness variation with 20 N applied. After voltage removal, when 10 N are applied, the pressure is not sufficient to force out the gas from the porosity of the separator and, indeed the thickness remains constant. On the other hand, the 20 N applied force leads to gas release from the separator, which results in continuous thickness decrease.

Graphite was then tested in PC-1 M LiTFSI in exfoliation condition with 10 N and 20 N applied. The dilatometer cell underwent a linear sweep voltammetry experiment from -0.1 V (open circuit potential) to - 4 V. The cell was discharged later and after a few hours underwent three CV cycles. The thickness variation was continuously monitored during the whole experiment as shown in Figure 6a. At the cell voltage of -2.5 V (≈ 0.9 V vs Li^+/Li) co-intercalation of $Li^+(PC)_n$ occurs. The dilatometric curve records a large expansion in electrode thickness (10-

12 μm) that represents a 35% change in thickness upon intercalation. This variation is consistent with the co-intercalation of $Li^+(PC)_n$ and corresponding exfoliation of the graphite. The related linear sweep voltammetry (Figure S4a) appears noisy due to gas evolution originating from the reductive degradation of PC in propylene [30, 31]. Consequently, in addition to the intercalation of solvated lithium ions in the material, the formation of propylene gas causes crack and exfoliation of the graphite layers. The resultant dilatometric curve (Figure 6a) is given by the combination of the exfoliation and the gas evolution.

The force adjustment system and the control of the applied pressure allow to get insight into the contribution of the gas formation during the expansion as shown before for H_2 evolution, and Figure 6b displays the thickness variation of the cell operating in exfoliation condition with 20 N applied force. The expansion decrease was observed, as expected. The first cycle expansion corresponds to 13 μm and 8 μm for 10 N and 20 N experiments, respectively. The pore volume filled by the evolved gas is smaller when external high force is applied and, in turn, the recorded expansion.

3.5 Chemical-physical characterization

SEM measurements were carried out on the graphite electrodes to get information about the consequences of the cycling (ten CVs) and of the applied force. Figure 7 depicts the SEM images of the pristine graphite electrode (Figure 7a) and of the graphite electrodes after cycling in the two electrolytic mixtures (Figure 7b and 7c). While from SEM images it is difficult to realize the difference between the pristine graphite electrode and the one cycled in EC: DMC (Figure 7b), the exfoliation of the electrode cycled in PC is evident on the bottom-left corner of the image (Figure 7c) in which expanded graphitic layers are visible.

Raman spectroscopy was used as a very effective way to investigate the bonding structure of graphite before cycling and the modification due to the cycling in the two electrolytes. The

Raman spectra of the graphite after cycling with 10 N force applied by the dilatometer were recorded and compared to the spectrum of the pristine electrode material (Figure 8). Samples rest 20 hours inside the electrochemical chamber of the dilatometer under a force applied of 10 N in two electrolytes to reach complete dimensional stability.

The characteristic graphite D, G, and 2D bands are present at 1350, 1580, and 2450 cm^{-1}, respectively. Additionally, the Raman spectrum of the pristine graphite spectrum shows a peak at 1564 cm^{-1} related to the D' band [32].

The graphite tested in LP30 evidenced the SEI formation only after cycling attributed to the peaks present in the low-frequency region of the spectrum in Figure 8a. The spectrum of the graphite before cycling in PC in Figure 8b also displays an additional peak that could be ascribed to an uncompleted removal of PC from the electrode. After cycling in PC in exfoliation condition, the D band in the Raman spectrum of graphite decreases, and the spectrum appears similar to that of the high ordered graphite [33]. The co-intercalation of PC molecules gradually damages the electrode and causes cracks and exfoliation of graphitic particles and, amorphous and small-sized carbon particles are the first to be detached from the electrode. The graphene sheets obtained were not detectable in the spectrum because of the washing step done on the material before recording the spectrum. Hence, only less damaged graphite particles remain attached to the current collector.

Ex situ XRD analyses of the samples after lithium ion intercalation have been also carried out. The details are reported in Supplementary Information (Figures S6-S7). However, ex situ XRD analyses is not suitable to correlate interlayer spacing and the dilatometric response, and in situ XRD characterization is necessary to this purpose.

4. Conclusions

The investigation of the volumetric stability of electrodes through ageing simulations is fundamental to predict the lifetime and the long-term stability of the cell. In the present study, a novel in situ dilatometer equipped with a system of force regulation was evaluated with model electrodes sustaining various electrochemical processes. The thickness variation of the graphite electrode in EC: DMC-based electrolyte revealed simultaneous processes (insertion/deinsertion, solvent evaporation, SEI formation and gas evolution). In the PC-based electrolyte, the uncompleted Li^+ intercalation in the lattice limits the exfoliation and the related damages to the graphite. On the contrary, the dramatic exfoliation of the electrode occurs when complete Li^+ intercalation takes place assisted by PC degradation and the formation of propene.

At the constant temperature, the variation of an external force is extremely useful in distinguishing different phenomena such as solvent evaporation, which could be responsible of the capacity fading, or gassing process. However, the applied force should not be so high to cause material deformation during measurements, or if high force is needed, the test should start after a resting time that assures the system components have reached their stable dimension. It has been demonstrated that this equipment can provide significant practical information on the behaviour of the cell, taking into account all its components, and also of the electrodes. However, future studies will be done with the new cell holder (under development) for a deeper understanding of the individual electrode behaviour.

Acknowledgements

The research was carried out in the framework of an Agreement between the University of Bologna and Marposs SpA that kindly provided the equipment for dilatometry tests to the Laboratory of Electrochemistry of Materials for Energetics, Department of Chemistry "Giacomo Ciamician".

References

[1] B. Dunn, H. Kamath, J.M. Tarascon, Electrical energy storage for the grid: A battery of choices, Science (80-.). 334 (2011) 928–935. https://doi.org/10.1126/science.1212741.

[2] A. Yamada, Iron-based materials strategies, MRS Bull. 39 (2014) 423–428. https://doi.org/10.1557/mrs.2014.89.

[3] M. Winter, G.H. Wrodnigg, J.O. Besenhard, W. Biberacher, P. Novák, Dilatometric Investigations of Graphite Electrodes in Nonaqueous Lithium Battery Electrolytes, J. Electrochem. Soc. 147 (2000) 2427. https://doi.org/10.1149/1.1393548.

[4] V.L. Chevrier, G. Ceder, Challenges for Na-ion Negative Electrodes, J. Electrochem. Soc. 158 (2011) A1011. https://doi.org/10.1149/1.3607983.

[5] B. Rieger, S. Schlueter, S. V. Erhard, J. Schmalz, G. Reinhart, A. Jossen, Multi-scale investigation of thickness changes in a commercial pouch type lithium-ion battery, J. Energy Storage. 6 (2016) 213–221. https://doi.org/10.1016/j.est.2016.01.006.

[6] J.-S. Bridel, T. Azaïs, M. Morcrette, J.-M. Tarascon, D. Larcher, In Situ Observation and Long-Term Reactivity of Si/C/CMC Composites Electrodes for Li-Ion Batteries, J. Electrochem. Soc. 158 (2011) A750. https://doi.org/10.1149/1.3581024.

[7] M. Li, Z. Wang, J. Fu, K. Ma, E. Detsi, In situ electrochemical dilatometry study of capacity fading in nanoporous Ge-based Na-ion battery anodes, Scr. Mater. 164 (2019) 52–56. https://doi.org/10.1016/j.scriptamat.2019.01.030.

[8] G. Jeong, S.M. Lee, N.S. Choi, Y.U. Kim, C.K. Lee, Stabilizing dimensional changes in Si-based composite electrodes by controlling the electrode porosity: An in situ electrochemical dilatometric study, Electrochim. Acta. 56 (2011) 5095–5101. https://doi.org/10.1016/j.electacta.2011.03.071.

[9] D. Sauerteig, S. Ivanov, H. Reinshagen, A. Bund, Reversible and irreversible dilation of lithium-ion battery electrodes investigated by in-situ dilatometry, J. Power Sources. 342 (2017) 939–946. https://doi.org/10.1016/j.jpowsour.2016.12.121.

[10] R. Kumar, J.H. Woo, X. Xiao, B.W. Sheldon, Internal Microstructural Changes and Stress Evolution in Silicon Nanoparticle Based Composite Electrodes, J. Electrochem. Soc. 164 (2017) A3750–A3765. https://doi.org/10.1149/2.0951714jes.

[11] M. Li, Z. Wang, E. Detsi, In Situ Electrochemical Dilatometry Study of (De)lithiation and Polysulfide Dissolution-Induced Dimensional Changes in Lithium-Sulfur Cathodes during Charging and Discharging, J. Electrochem. Soc. 167 (2020) 050505. https://doi.org/10.1149/1945-7111/ab63c1.

[12] P.K. Nayak, L. Yang, K. Pollok, F. Langenhorst, D. Aurbach, P. Adelhelm, Investigation of Li1.17Ni0.20Mn0.53Co0.10O2 as an Interesting Li- and Mn-Rich Layered Oxide Cathode Material through Electrochemistry, Microscopy, and In Situ Electrochemical Dilatometry, ChemElectroChem. 6 (2019) 2812–2819. https://doi.org/10.1002/celc.201900453.

[13] T. Kim, S. Park, S.M. Oh, Solid-State NMR and Electrochemical Dilatometry Study on Li[sup +] Uptake/Extraction Mechanism in SiO Electrode, J. Electrochem. Soc. 154 (2007) A1112. https://doi.org/10.1149/1.2790282.

[14] M. Hahn, H. Buqa, P.W. Ruch, D. Goers, M.E. Spahr, J. Ufheil, P. Novák, R. Kötz, A dilatometric study of lithium intercalation into powder-type graphite electrodes, Electrochem. Solid-State Lett. 11 (2008) 150–154. https://doi.org/10.1149/1.2940573.

[15] A. Tranchot, H. Idrissi, P.X. Thivel, L. Roué, Impact of the Slurry pH on the Expansion/Contraction Behavior of Silicon/Carbon/Carboxymethylcellulose Electrodes for Li-Ion Batteries, J. Electrochem. Soc. 163 (2016) A1020–A1026.

https://doi.org/10.1149/2.1071606jes.

[16] V.R. Rikka, S.R. Sahu, A. Chatterjee, P. V. Satyam, R. Prakash, M.S.R. Rao, R. Gopalan, G. Sundararajan, In Situ/ex Situ Investigations on the Formation of the Mosaic Solid Electrolyte Interface Layer on Graphite Anode for Lithium-Ion Batteries, J. Phys. Chem. C. 122 (2018) 28717–28726. https://doi.org/10.1021/acs.jpcc.8b09210.

[17] M. Nagayama, K. Ariyoshi, Y. Yamamoto, T. Ohzuku, Characterization of Lithium Insertion Electrodes by Precision Dilatometer: Area-Specific Deformation of Single Electrode, J. Electrochem. Soc., 161 (2014) A1388-A1393. https://doi.org/10.1149/2.0981409jes

[18] T. Ohzuku, N. Matoba, K. Sewai, Direct evidence on anomalous expansion of graphite-negative electrodes on first charge by dilatometry, J. Power Sources 97-98 (2001) 73-77.

[19] J.P. Pender, G. Jha, D.H. Youn, J.M. Ziegler, I. Andoni, E.J. Choi, A. Heller, B.S. Dunn, P.S. Weiss, R.M. Penner, C.B. Mullins, Electrode Degradation in Lithium-Ion Batteries, ACS Nano. 14 (2020) 1243–1295. https://doi.org/10.1021/acsnano.9b04365.

[20] M. Winter, J.O. Besenhard, M.E. Spahr, P. Novák, Insertion electrode materials for rechargeable lithium batteries, Adv. Mater. 10 (1998) 725–763. https://doi.org/10.1002/(SICI)1521-4095(199807)10:10<725::AID-ADMA725>3.0.CO;2-Z.

[21] G.-C. Chung, H.-J. Kim, S.-I. Yu, S.-H. Jun, J. Choi, M.-H. Kim, Origin of Graphite Exfoliation An Investigation of the Important Role of Solvent Cointercalation, J. Electrochem. Soc. 147 (2000) 4391. https://doi.org/10.1149/1.1394076.

[22] H.Y. Song, S.K. Jeong, Investigating continuous co-intercalation of solvated lithium ions and graphite exfoliation in propylene carbonate-based electrolyte solutions, J. Power

Sources. 373 (2018) 110–118. https://doi.org/10.1016/j.jpowsour.2017.11.015.

[23] M. Onuki, Y. Sakata, M. Yanagidate, Y. Otake, S. Kinoshita, M. Ue, M. Deguchi, Identification of the Source of Evolved Gas in Li-Ion Batteries by Using 13C-Labeled Solvents, ECS Trans. 11 (2019) 43–47. https://doi.org/10.1149/1.2897970.

[24] T. Liu, L. Lin, X. Bi, L. Tian, K. Yang, J. Liu, M. Li, Z. Chen, J. Lu, K. Amine, K. Xu, F. Pan, In situ quantification of interphasial chemistry in Li-ion battery, Nat. Nanotechnol. 14 (2019) 50–56. https://doi.org/10.1038/s41565-018-0284-y.

[25] L. Wang, A. Menakath, F. Han, Y. Wang, P.Y. Zavalij, K.J. Gaskell, O. Borodin, D. Iuga, S.P. Brown, C. Wang, K. Xu, B.W. Eichhorn, Identifying the components of the solid–electrolyte interphase in Li-ion batteries, Nat. Chem. 11 (2019) 789–796. https://doi.org/10.1038/s41557-019-0304-z.

[26] B. Strehle, S. Solchenbach, M. Metzger, K.U. Schwenke, H.A. Gasteiger, The Effect of CO 2 on Alkyl Carbonate Trans-Esterification during Formation of Graphite Electrodes in Li-Ion Batteries, J. Electrochem. Soc. 164 (2017) A2513–A2526. https://doi.org/10.1149/2.1001712jes.

[27] J.S. Shin, C.H. Han, U.H. Jung, S.I. Lee, H.J. Kim, K. Kim, Effect of Li2CO3 additive on gas generation in lithium-ion batteries, J. Power Sources. 109 (2002) 47–52. https://doi.org/10.1016/S0378-7753(02)00039-3.

[28] R. Bernhard, M. Metzger, H.A. Gasteiger, Gas Evolution at Graphite Anodes Depending on Electrolyte Water Content and SEI Quality Studied by On-Line Electrochemical Mass Spectrometry, J. Electrochem. Soc. 162 (2015) A1984–A1989. https://doi.org/10.1149/2.0191510jes.

[29] B. Michalak, H. Sommer, D. Mannes, A. Kaestner, T. Brezesinski, J. Janek, Gas Evolution in Operating Lithium-Ion Batteries Studied in Situ by Neutron Imaging, Sci.

Rep. 5 (2015) 1–9. https://doi.org/10.1038/srep15627.

[30] M.R. Wagner, P.R. Raimann, A. Trifonova, K.C. Möller, J.O. Besenhard, M. Winter, Dilatometric and mass spectrometric investigations on lithium ion battery anode materials, in: Anal. Bioanal. Chem., Springer, 2004: pp. 272–276. https://doi.org/10.1007/s00216-004-2570-9.

[31] M. Hahn, A. Würsig, R. Gallay, P. Novák, R. Kötz, Gas evolution in activated carbon/propylene carbonate based double-layer capacitors, Electrochem. Commun. 7 (2005) 925–930. https://doi.org/10.1016/j.elecom.2005.06.015.

[32] C. Srilakshmi, E. Widjaja, M. Garland, B.G. Anderson, Deconvolution of pure component FT-Raman spectra from thermal emission of barium sulfate and graphite samples using the BTEM algorithm, J. Raman Spectrosc. 38 (2007) 349–355. https://doi.org/10.1002/jrs.1652.

[33] P.K. Chu, L. Li, Characterization of amorphous and nanocrystalline carbon films, Mater. Chem. Phys. 96 (2006) 253–277. https://doi.org/10.1016/j.matchemphys.2005.07.048.

Figure and Scheme captions

Figure 1. Marposs electrochemical dilatometer with electronic control unit.

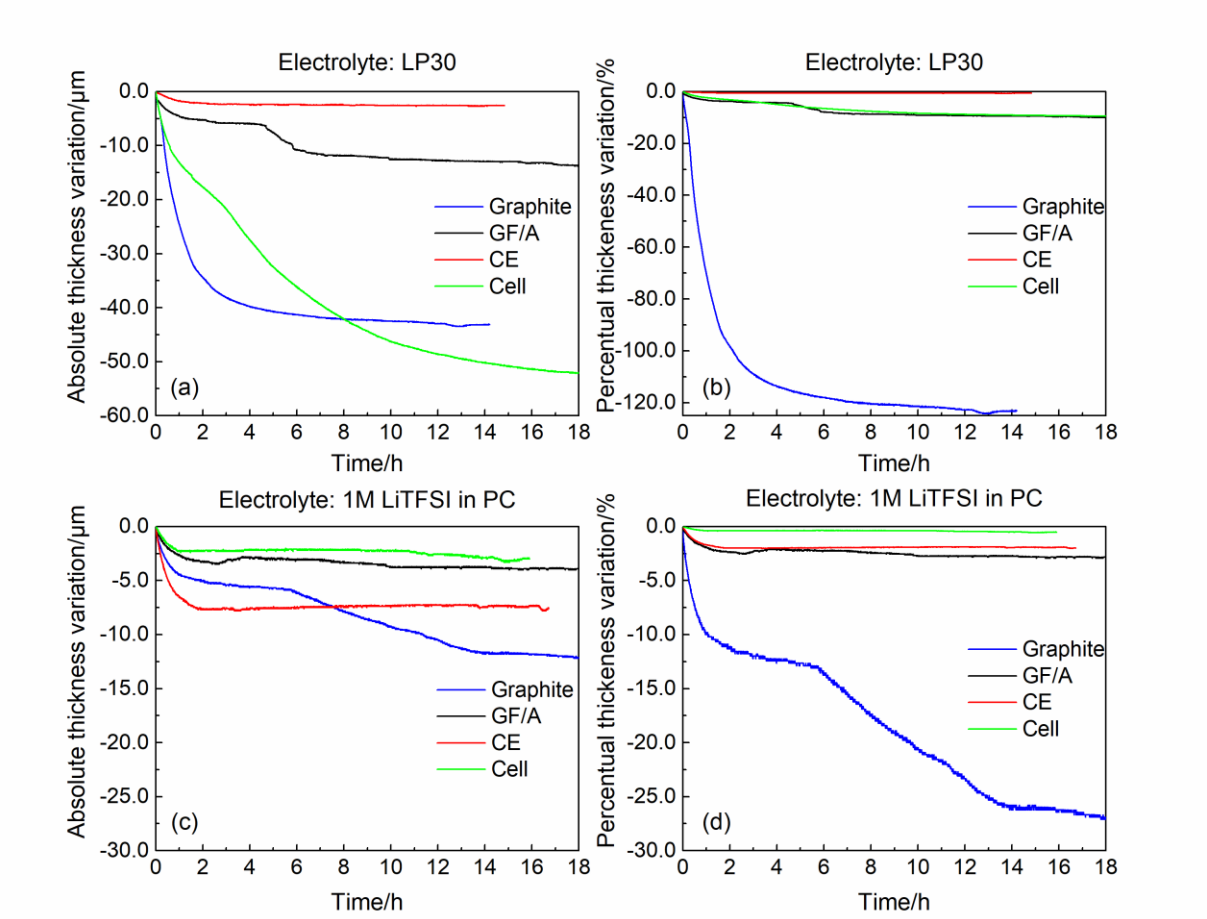

Figure 2. Absolute (a, c) and percentual (b, d) deformation of cell components and of the whole cell under 10 N force with different electrolytes, LP30 (a,b) and PC-1M LiTFSI (c,d).

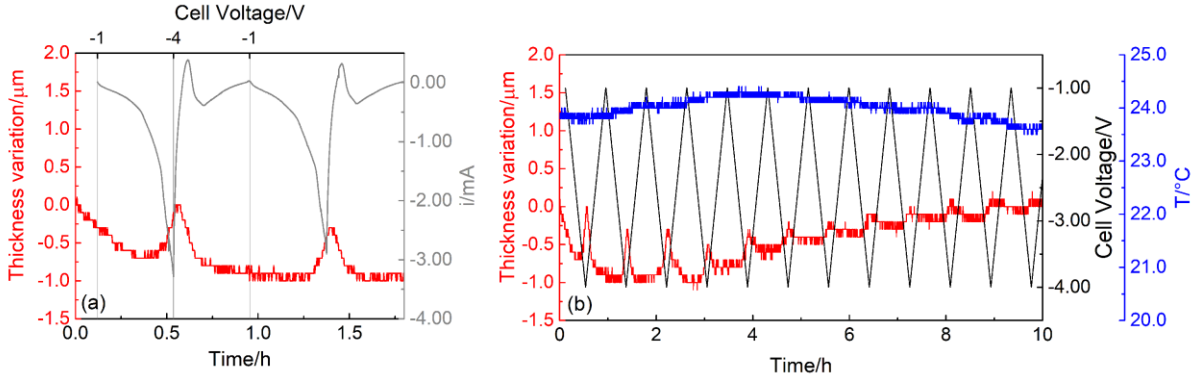

Figure 3. (a) Thickness variation (red) and current (gray) during the first two CVs of the graphite//CE in dilatometer cell (2 mV s^{-1}); (b) thickness variation (red), voltage (black) and temperature (blue) during 10 continuous CVs of the graphite//CE in dilatometer cell (2 mVs^{-1})

WE: graphite, CE-RE: activated carbon, separator Whatmann: GF/A, WE: graphite, CE-RE: activated carbon, separator Whatmann: GF/A, 150 µL LP30.

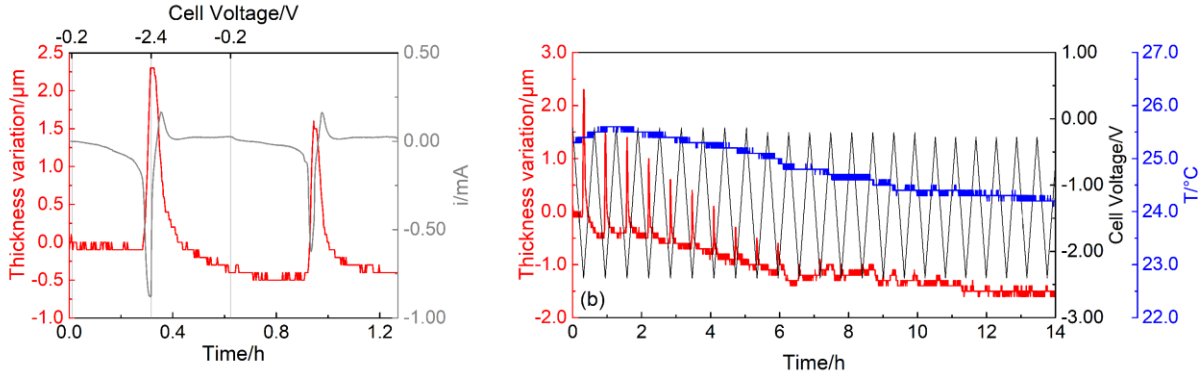

Figure 4. (a) Thickness variation (red) and current (gray) during the first two CVs of the graphite//CE in dilatometer cell (2 mV s^{-1}); (b) thickness variation (red), voltage (black) and temperature (blue) during 10 continuous CVs of the graphite//CE in dilatometer cell (2 mVs^{-1})

WE: graphite, CE-RE: activated carbon, separator Whatmann: GF/A, 150 µL PC- 1M LiTFSI.

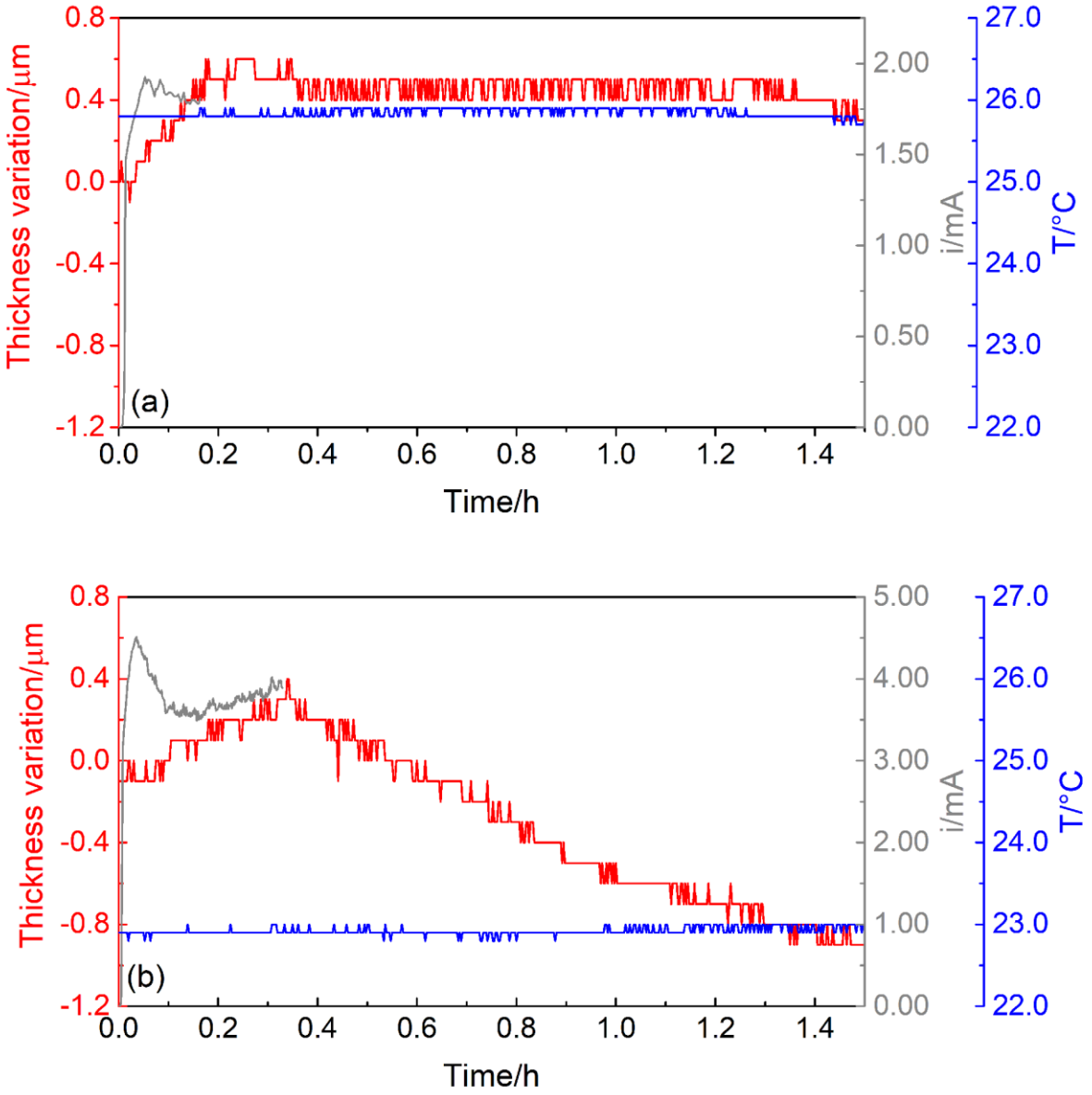

Figure 5. Thickness variation during hydrogen evolution (red) under an applied potential of 1V in 1 M NaCl aqueous solution, current (gray) and temperature (blue). WE: Platinum 10 mm diameter, Separator Whatman GF/A, CE-RE: Platinum 8 mm diameter, 350 µL 1M NaCl in H_2O. (a) 10 N and (b) 20 N applied force.

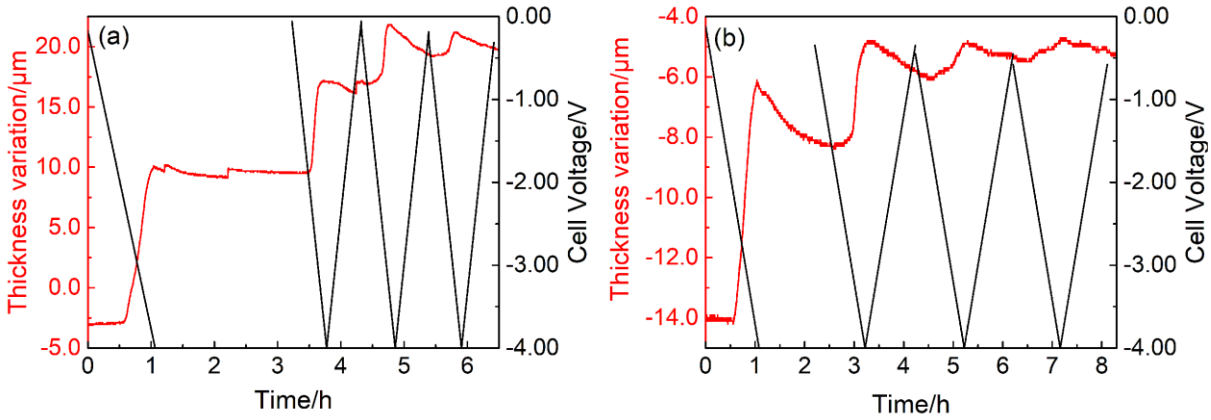

Figure 6. Thickness variation (red) and cell voltage (black) during electrochemical experiments under (a) 10 N and (b) 20 N applied force. WE: graphite, CE-RE: activated carbon, separator Whatman: GF/A, 150 µL PC -1 M LiTFSI.

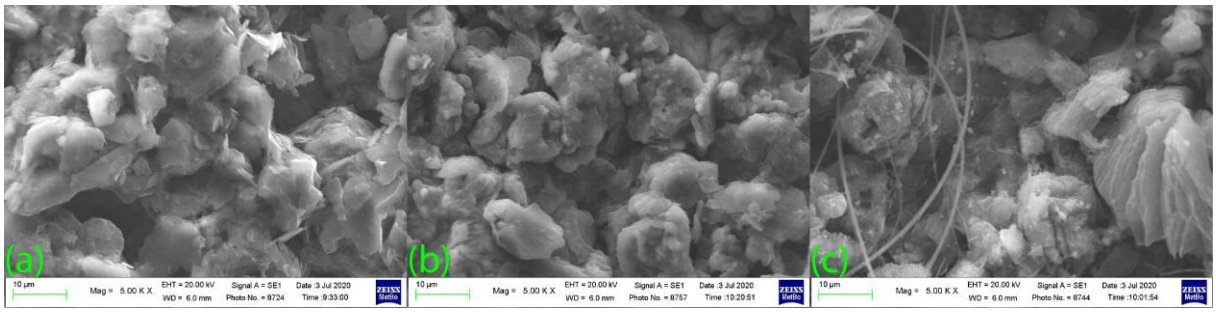

Figure 7. SEM images of (a) pristine graphite electrode, (b) graphite electrode cycled in LP30 and (c) graphite electrode cycled in exfoliation condition in PC-1M LiTFSI.

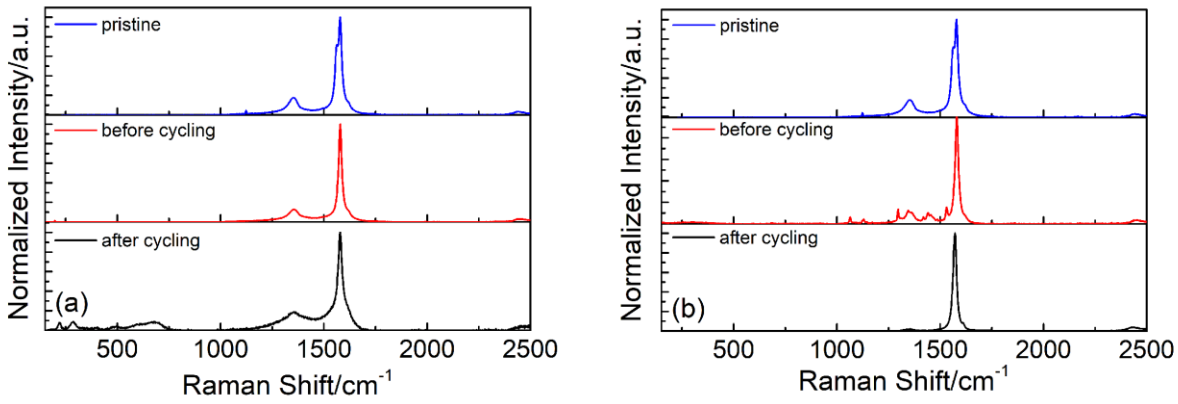

Figure 8. Raman spectrum of graphite electrode before and after cycling (a) in LP30 and (b) in PC - 1M LiTFSI.

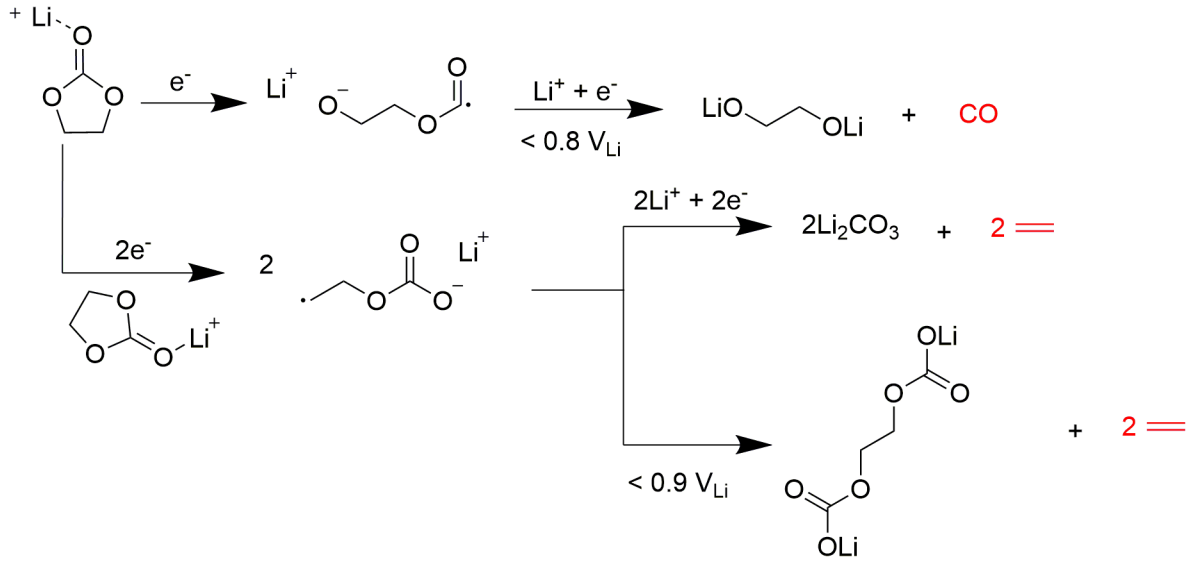

Scheme 1. Possible reductive degradation pathways of EC with gas phase co-product (red labelled).

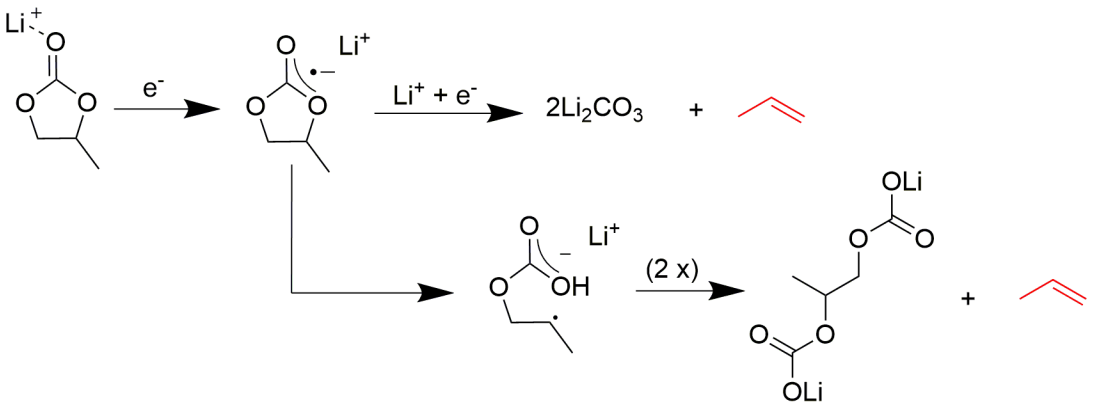

Scheme 2. Possible reductive degradation pathways of PC with gas phase co-product (red labelled).

Supplementary information

Electrodilatometric analysis under applied force: a powerful tool for electrode investigation

Giampaolo Lacarbonara[a,§], Morteza Rahmanipour[a,#,§], Juri Belcari[b,c], Lorenzo Lodi[c], Andrea Zucchelli[b], Catia Arbizzani[a,*,§]

[a]Alma Mater Studiorum - University of Bologna, Dept. of Chemistry "Giacomo Ciamician", Via F. Selmi 2, 40126 Bologna, Italy

[b]Alma Mater studiorum - Engineering School, Industrial Engineering Department (DIN), Viale del Risorgimento 2, 30136, Bologna, Italy

[c]Marposs Spa Italy, Via Saliceto, 13, 40010 Bentivoglio (Bo), Italy

* Corresponding Author: catia.arbizzani@unibo.it

§ ISE Members

Present address: Manz Italy Srl, Via S. Lorenzo, 19, 40037 Sasso Marconi (BO), Italy

1. T-shaped cell experiments

Given that the dilatometer cell works in two electrode mode and an activated carbon electrode was selected as counterelectrode (CE) /reference electrode (RE), it is mandatory to evaluate the potential range of the processes in a T-shaped cell operating in two-electrode mode with the monitoring of the electrode potentials vs. a reference Li electrode, and to verify the reproducibility of the experiments in the dilatometer cell. After assembly, the potentials were measured versus an internal lithium metal reference electrode. In LP30 electrolyte, the open-circuit potential (OCP) was -40 mV that corresponds to 3.40 V vs Li^+/Li for the anode and 3.44 V vs Li^+/Li for the cathode. Considering that the two electrodes have similar potential, cyclic voltammetries (CV) have been performed at 2 mV s^{-1} from the OCP to increasingly negative potential (Figure S1). The voltammograms show the typical profile associated with the redox process of the graphite during insertion/deinsertion of lithium ions in the layers of graphite. In the first cycle is evident the reduction process of EC to produce the SEI. The potentials of each electrode vs. lithium metal RE were reported in Table S1. At - 4 V the potentials of the anode and the cathode were 50 mV vs Li^+/Li and 4.05 V vs Li^+/Li, respectively. Hence, - 4 V was chosen as the limit for the CV experiments. The electrode potential values recorded during CVs in PC-1M LiTFSI ar

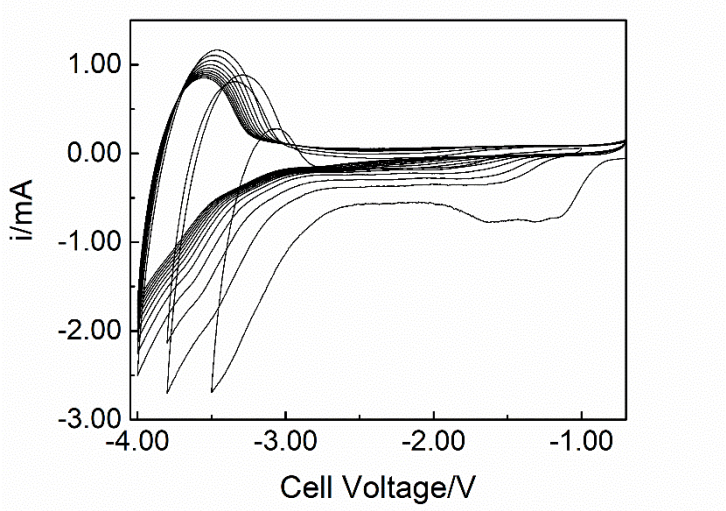

Figure S1. Preliminary CV experiments in LP30 (2 mV s^{-1}) in a T-shaped cell. The CV were carried out in two electrode mode, but the graphite WE and activated carbon CE potentials were monitored and measured vs lithium RE. The potential values are reported in Table S1.

Table S1. Graphite (G) and activated carbon (AC) electrode potentials measured vs lithium RE in the T-shaped cell.

Cell Voltage (V)	E_G (V) vs Li^+/Li	E_{AC} (V) vs Li^+/Li
-0.04	3.40	3.44
-1.00	2.05	3.05
-2.00	1.18	3.18
-2.50	0.84	3.34
-3.00	0.59	3.59
-3.50	0.38	3.87
-3.80	0.15	3.95
-4.00	0.05	4.05

2. Thickness variation data

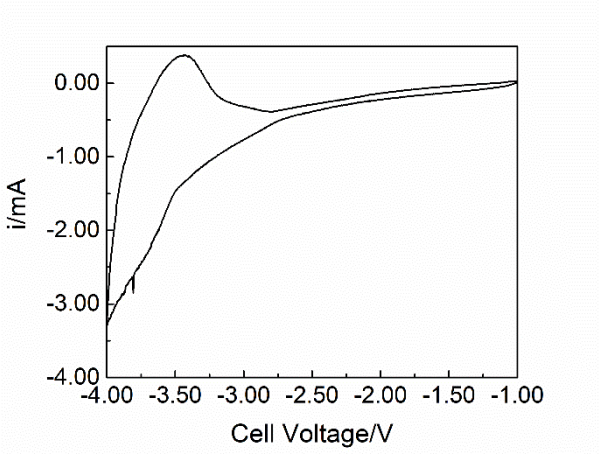

Figure S2. CV (2nd cycle) at 2 mV s^{-1} WE: graphite, CE-R: activated carbon, separator Whatman: GF/A, 150 µL LP30.

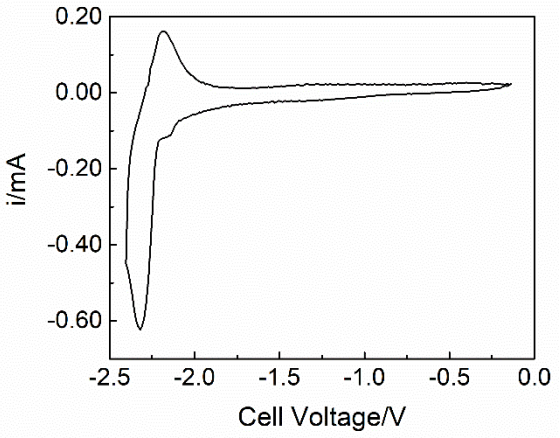

Figure S3. CV (2nd cycle) at 2 mV s^{-1} in WE: graphite, CE-R: activated carbon, separator Whatman: GF/A, 150 µL PC-1M LiTFSI.

3. Variable force experiments

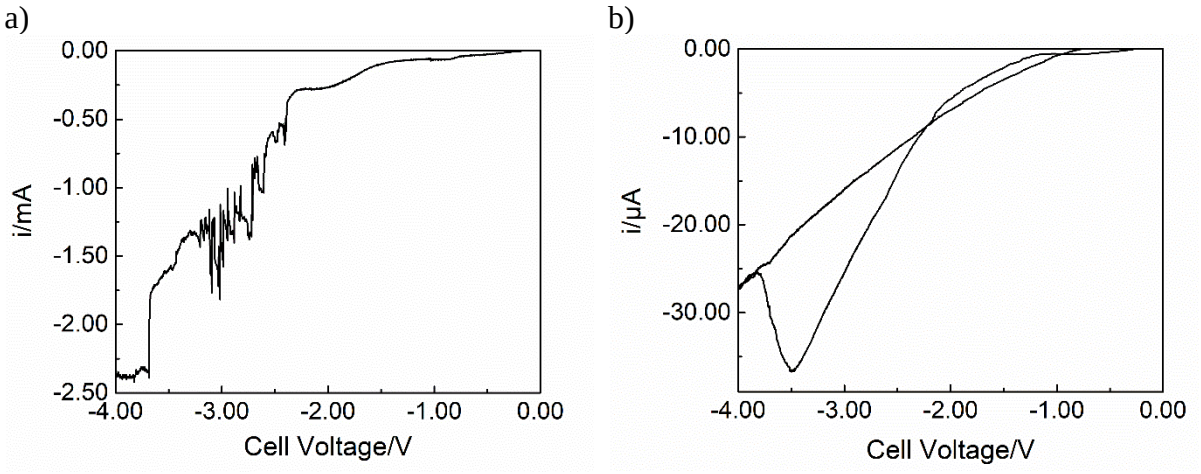

Figura S4. Electrochemical tests under 10 N applied force; a) linear sweep voltammetry from OCP to -4 V, 1 mV s^{-1}; b) 1st CV from OCV to -4 V, 1 mV s^{-1}. WE: graphite, CE-R: activated carbon, separator Whatman: GF/A, 150 µL PC-1 M LiTFSI.

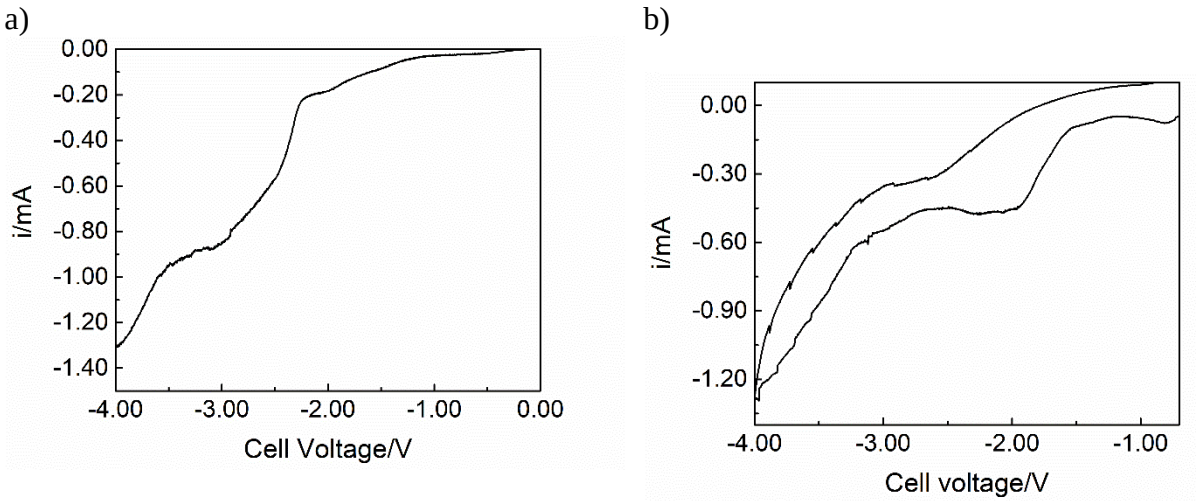

Figure S5. Electrochemical tests under 20 N applied force; a) linear sweep voltammetry from OCP to -4 V, 1 mV s^{-1}; b) 1st CV from OCV to -4 V, 1 mV s^{-1}. WE: graphite, CE-R: activated carbon, separator Whatman: GF/A, 150 µL PC- 1 M LiTFSI.

4. Ex situ XRD analysis

X-ray diffraction (XRD) experiments on samples that were cycled in the dilatometer. XRD data were obtained by using an x-ray diffractometer PANalytical X'Pert PRO (Malvern Panalytical, United Kingdom) equipped with an X'Celerator detector (Cu K_α radiation, 40 mA, 40 kV). The spectra were acquired at detection angles of 26° and 45° in which (002) and (004) interlayer associated reflections of the graphite are visible. The XRD analysis was carried after linear sweep voltammetry (LSV), in two electrode mode, with activated carbon as counter and reference electrode and graphite as the working electrode (≈2.5 mg cm^{-2}) in the electrochemical chamber of the dilatometer under an applied force of 10 N. After cycling, the electrodes were washed with DMC and stored in dry box. The XRD samples were sealed in dry box between a microscope slide and a mylar protective film to preserve the Ar atmosphere during the analysis. Pristine electrodes were prepared by pressing in the electrochemical chamber of the dilatometer at 10N for 2h without electrolyte.

The Figure S6 shows the reflexes (002), (004), for which $2\theta \approx 26.7, 54.8°$, respectively, for the sample tested in LP30. The diffraction reflexes' asymmetry indicates several carbon phases (substructures) with different degrees of order and structural characteristics [1].

As shown in the Figure S6, in LP30, the dilatometric signal is complicated by the evaporation of the DMC and the SEI formation.

Pristine graphite showed the (002) reflection at 26.69° (d = 3.33 Å), while the electrode dipped in LP30 (red curve in Figure 1) showed a peak at 26.57° associated with the presence of EC left after the DMC washing, also confirmed by the presence of a reflection at 16.81°[2].

During the charge, the dilatometric response showed an expansion of 0.3 and 0.5 μm, for 40 and 65% SOCs, respectively (Figure S7). In the diffractograms, a small reflection shift toward lower angle ($d_{40\%}$ = 3.358 Å, $d_{65\%}$ = 3,360 Å) is visible. The shift observed results coherent

with the shift expected for partially lithiated graphite but 40-60% SOCs should correspond the presence of stage 2-stage 3 graphite phases and an increase of the interlayer spacing of 0.1-0.2 Å [3]. Analogous response was obtained for the samples tested in PC-1 LiTFSI.

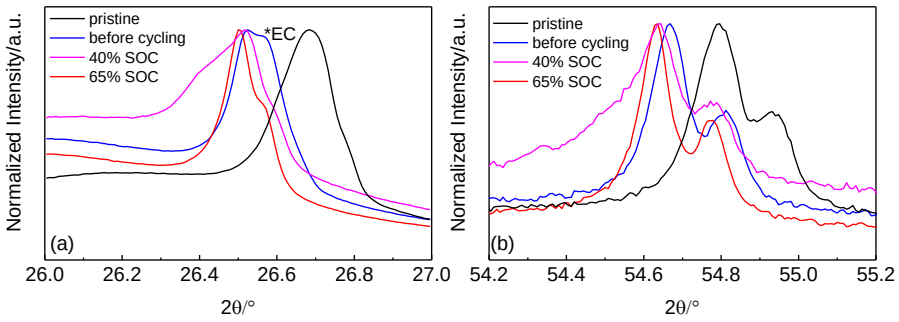

Figure S6. XRD diffractogram of (002) and (004) reflection in LP30.

In addition, as discussed in Section 3.1, the dilatometer pressure leads to a material deformation that modifies the electrode height. Figure S8 shows the influence of the pressure applied by the dilatometer on the diffractogram of the same dry electrode before and after press 2h at 10 N without cycling.

Also, as shown by Hahn et al., the dimensional change of the electrode during the formation of Li_xC_6 phases is minimal for x= 0.2 and 0.6, in agreement with only small changes detected by X-ray diffraction [4]

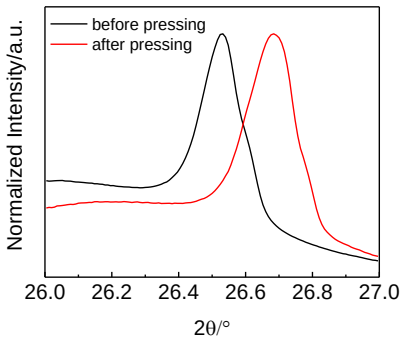

Figure S7. XRD diffractogram of (002) reflection of pristine graphite before and after pressing the electrode at 10N for 2h without electrolyte.

[1] Popova A. N., Crystallographic Analysis of Graphitw by X-Ray Diffraction, Coke and Chemistry 60 (9) (2017), 361-365. http://doi.org/10.3103/S1068364X17090058

[2] Peruzzi N., Ninham B. W., Lo Nostro P., Baglioni P., Hofmeister Phenomena in Nonaqueous Media: The Solubility of Electrolytes in Ethylene Carbonate, J. Phys. Chem. B 116 (2012), 14398−14405. https://dx.doi.org/10.1021/jp309157x

[3] Grimsmann F., Brauchle F., Gerbert T., Gruhle A., Knipper M., Parisi J., Hysteresis and current dependence of the thickness change of lithium-ion cells with graphite anode, Journal of Energy Storage 12 (2017) 132–137. http://dx.doi.org/10.1016/j.est.2017.04.006

[4] Hahn M., Buqa H., Ruch P. W., Goers D., Spahr M. E., Ufheil J., Novák P., Kötz R., A Dilatometric Study of Lithium Intercalation into Powder-Type Graphite Electrodes, Electrochemical and Solid-State Letters 11(9) (2008), A151-A154. http://doi.org/10.1149/1.2940573